Explanation for Twin Tunnelling-induced Surface Settlements by Changes in Soil Stiffness on Account of Stress History

Tianqi Zhang[1], R Neil Taylor[2], Sam Divall[2], Gang Zheng[1], Jibin Sun[1] Sarah Elizabeth Stallebrass[2], and Richard James Goodey[2]

[1]School of Civil Engineering, Tianjin University, Tianjin 300072, China.

[2]School of Engineering and Mathematical Sciences, City, University of London, Northampton Square, EC1V 0HB London, UK

Abstract: In this article, a group of representative centrifuge tests were selected for numerical modelling to explain the surface settlements induced by sequential twin tunnelling. Both Modified Cam Clay model (MCC) and Three-Surface Kinematic Hardening model (3-SKH) were adopted in the simulation, which indicated the use of 3-SKH model conduced to mimicking more closely centrifuge model response. Via performing more contrastive numerical analyses with 3-SKH model, the influence of the first tunnel event on the stiffness of the soil around the second tunnel was quantitatively investigated, whereby the mechanism behind the observed surface settlements was finally made clear.

Keywords: twin tunnelling; Modified Cam Clay model; Three-Surface Kinematic Hardening model; stiffness of soil

1. INTRODUCTION

Tunnels for mass transit systems are often constructed in pairs to facilitate travel in opposite directions. This arrangement is well known as twin-tunnelling. For the purpose of calculating settlements, O'Reilly and New (1982) suggested superposition of settlement profiles predicted for individual tunnels (Peck, 1969; Mair, 1979; Taylor, 1984). However, this simplified method was first challenged by field observations (Nyren, 1998; Cording and Hansmire, 1975; Cooper and Chapman, 1998; Cooper*et al.*, 2002; Fargnoli *et al.*, 2015), which showed that the surface settlements, in particular those generated by the second tunnel, would be potentially underestimated.

Chapman *el al.* (2007) performed 1 *g* physical model tests to investigate the ground movements subjected to the twin tunnel construction under controlled laboratory conditions. Greater surface settlements were shown to be generated by the second tunnel. This suggested that it ought to be the presence of the first tunnel influencing the behaviour of the second as other uncertainties in field sites can be excluded in the laboratory tests. Recently, Divall and Goodey (2012) further explored the twin tunnelling-induced ground movements using geotechnical centrifuge modelling as this technique guaranteed a correct stress distribution consistent with that of a prototype. Similarly, a relative increase in surface settlements due to the second tunnel was also observed. As equal volume loss was imposed for each tunnel, a

38 rationale behind such observations could be a reduced stiffness within certain areas of
39 soil mass (Divall and Goody, 2015). A further validation for this would be beyond the
40 capability of the physical model but may be investigated by numerical modelling
41 (Addenbrook, 1996), which could explore the stress paths around the second tunnel so
42 as to provide more information on any changes in soil stiffness and therefore a
43 understanding of the displacements (Divall, 2013).

44 In this article, numerical modelling, which was tailored for the above mentioned
45 centrifuge tests, was conducted with the experimental process carefully replicated, as
46 far as possible, so as to get an insight into what exactly happened during the tests. Both
47 a simple, but commonly used Modified Cam Clay (MCC) model (Roscoe and Burland,
48 1968) and an advanced Three-Surface Kinematic Hardening (3-SKH) model
49 (Stallebrass, 1990) were adopted in the course of the analyses. The predictive
50 capabilities of the two models were examined by a comparison against the test data,
51 making it possible to establish which features of the observed response can be
52 adequately reproduced by a simple elastoplastic model while others require complex
53 behaviour of the soil to be replicated. In this way, both the flaws of a MCC model and
54 the advantages of a 3-SKH model in simulating a twin tunnelling problem were made
55 clear. More importantly, as the constitutive framework of 3-SKH model was proposed
56 originally to simulate the effect of previous stress history on subsequent soil behaviour,

the changes in soil stiffness around the second tunnel due to the first can be investigated quantitatively. This provided a chance to explain in fundamental terms the characteristics of the observed surface settlements in the twin tunnelling centrifuge tests.

2. CENTRIFUGE TESTS

2.1 Brief Introduction

Three typical centrifuge tests, performed by Divall (2013) at City, University of London, were investigated in this article. A generic schematic of the centrifuge models can be seen in Fig. 1. The tests were in a plane strain configuration, only varying in tunnel centre to centre spacing (with a spacing S of 1.5D, 3.0D and 4.5D, respectively).

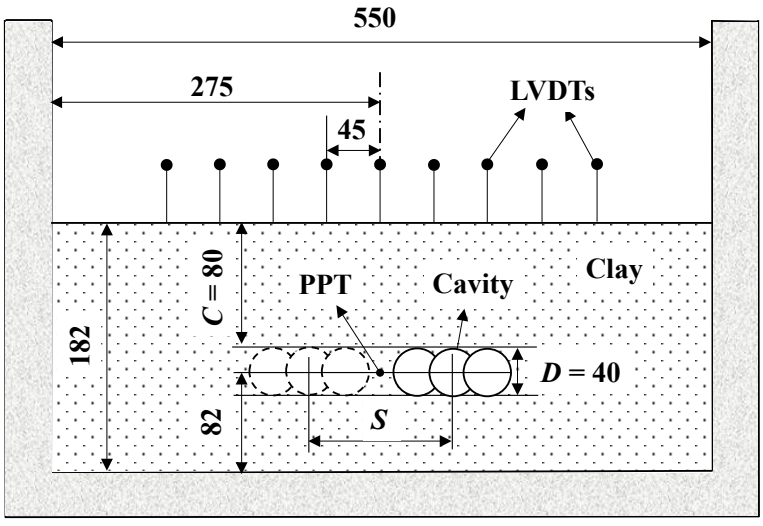

(a) Cross section view

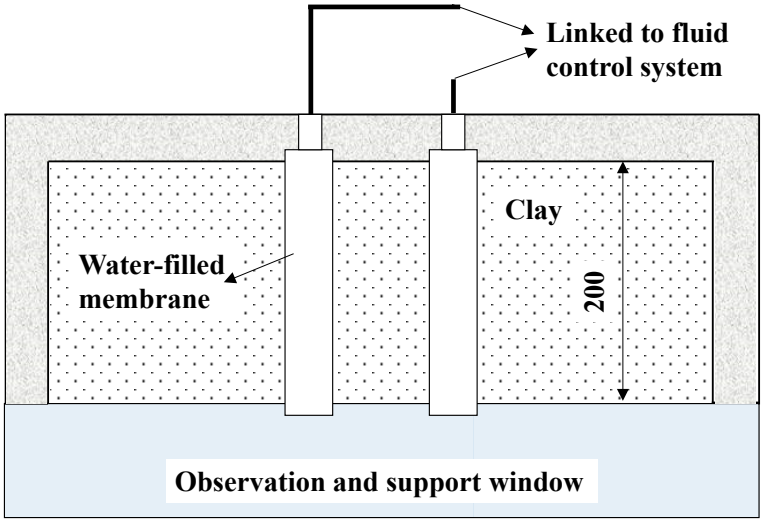

(b) Plan view

Fig. 1 Schematic of plane strain centrifuge models (Unit: mm)

Speswhite Kaolin clay slurry was consolidated in the centrifuge strong box to give a clay sample of being 550 mm wide, 182 mm high and 200mm thick. Two cylindrical cavities were cut in the sample and these would model the twin tunnels. The two cavities each had a diameter D of 40 mm and a cover C of 80 mm and were supported by water within a latex membrane. Volume loss due to tunnelling was simulated by extracting a predetermined volume of water from inside the latex membrane via a bishop ram equipped in the fluid control system. 9 Linear Variable Differential Transformers (LVDTs) were placed symmetrically about the model centre with a uniform spacing of 45mm to measure the surface settlements. One pore pressure transducer (PPT) was installed into the model at the midpoint between the two tunnels to measure the changes in pore pressure during the tests.

All the tests were carried out on models reduced by a scale factor N of 100 and accelerated to 100 g, following the centrifuge scaling laws (Schofield A,N., 1980). A flow chart of the experimental procedure can be seen in Fig. 2.

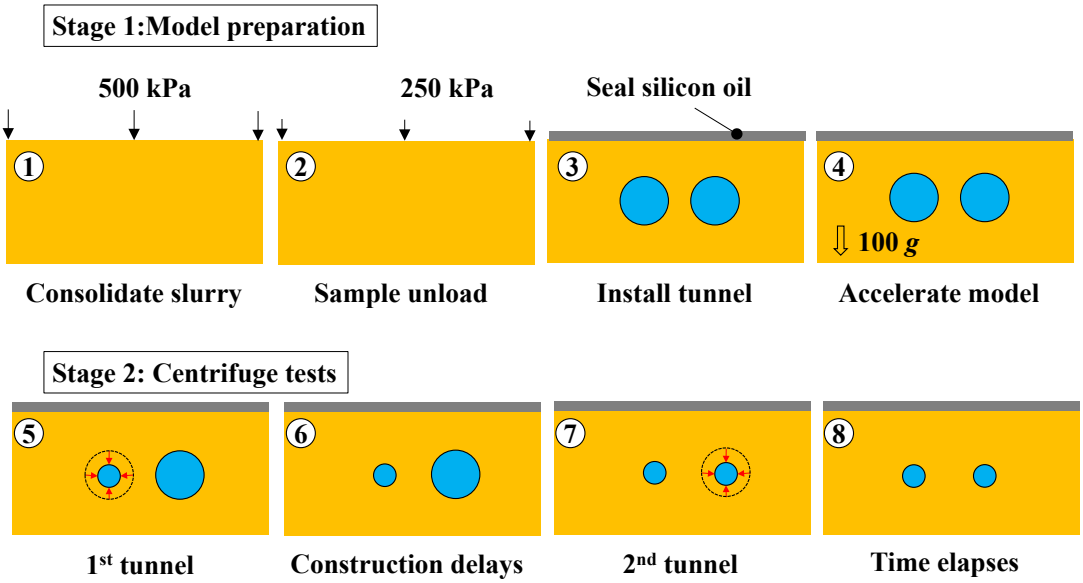

Fig. 2 Flow chart of experimental procedure

The experimental procedure can be divided into two stages:

Stage 1: Model preparation (include 4 steps)

Step 1: Consolidate slurry. The clay slurry with a water content of 120% was initially placed inside a rectangular container and consolidated one-dimensionally in a hydraulic press to achieve a desired stress history by consolidation to a vertical effective stress of 500 kPa.

Step 2: Sample unload. The vertical total stress was reduced so that the vertical effective stress decreased to 250 kPa after a period of swelling.

Step 3: Install tunnel. Once the sample was removed from the consolidation press, the exposed surface of clay was quickly sealed with silicon oil to prevent evaporation of water from the sample. Then the front-wall of the strong box was removed to gain access to the front clay surface, and approximately 4 hours were subsequently left for boring cavities and installing the tunnel apparatus.

Step 4: Accelerate model. Once the model making was completed, the assembled model was placed on the centrifuge swing, accelerated to 100 *g* within 4 minutes, and left running for 24 hours to achieve effective stress equilibrium.

Stage 2: Centrifuge tests (include 4 steps)

Step 5: First tunnel. Water was drained from the first tunnel within 60 seconds using the fluid control equipment to simulate the first tunnel construction. 7.54 ml of water was removed from the tunnel apparatus to achieve a volume loss of 3%.

Step 6: Construction delays. 3 minutes was left for the centrifuge to run before the second tunnel event, which represented a construction delay of 3 weeks at prototype scale according to the centrifuge scaling laws.

Step 7: Second tunnel. Same amount of water was removed from the second tunnel to simulate the second tunnel construction.

Step 8: Time elapses. The centrifuge was left to run for at least an hour post-test to allow longer term movements to develop.

2.2 Characteristics of observed surface settlements

Fig. 3 shows the observed surface settlements in the three tests.

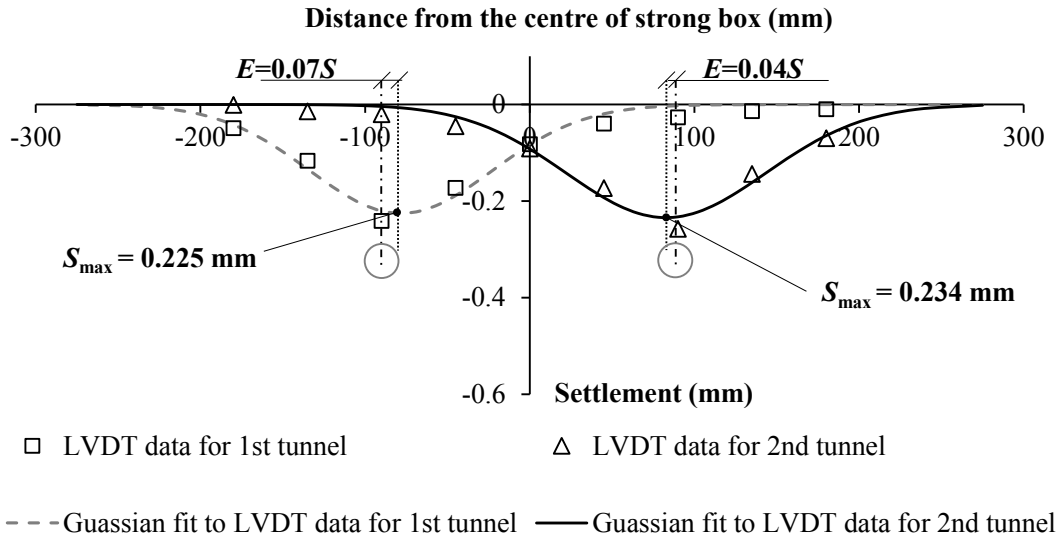

(a) $S = 4.5\ D$

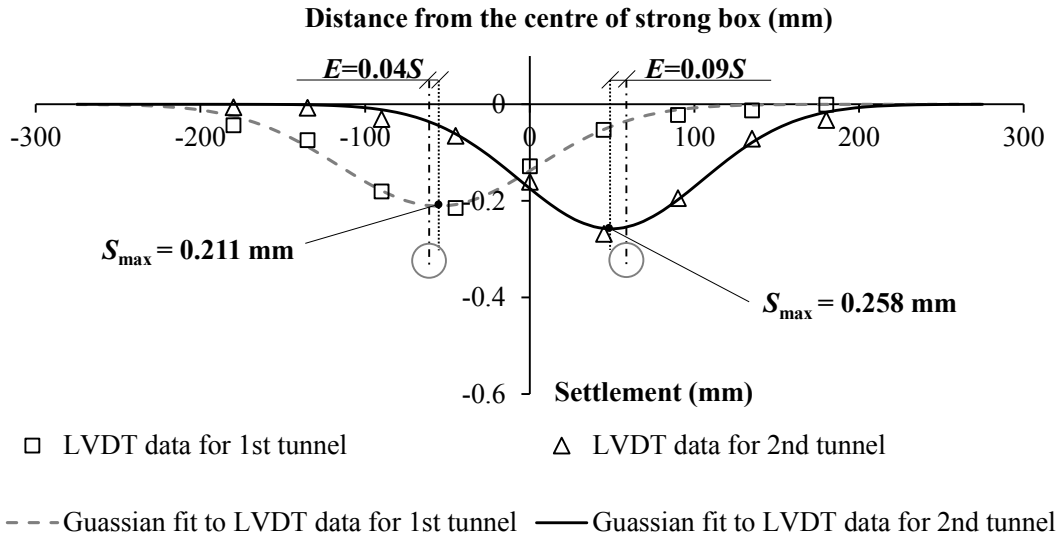

(b) $S = 3.0\ D$

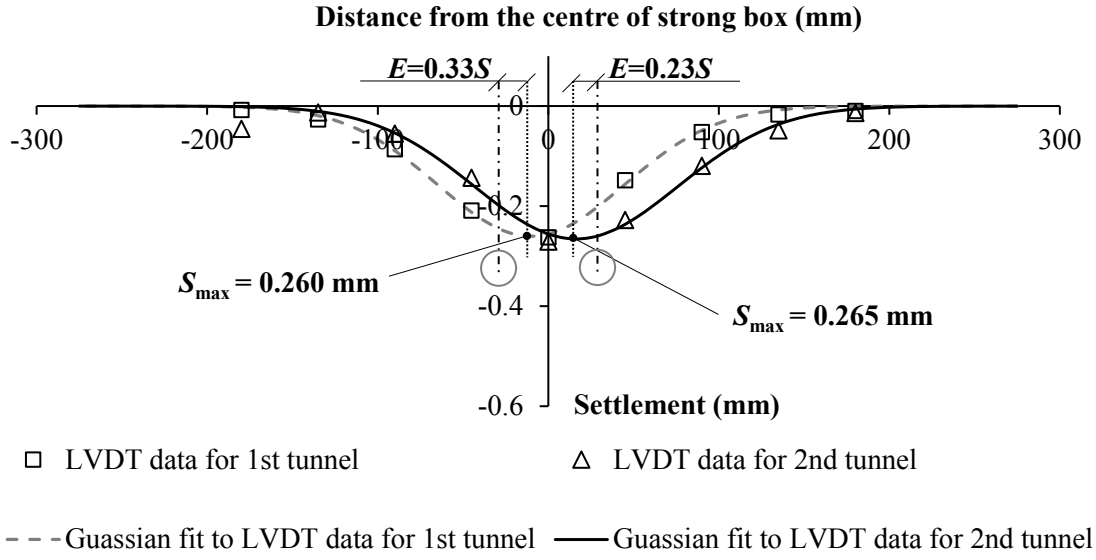

(c) $S = 1.5\ D$

Fig. 3 Observed surface settlements in three typical tests

Gaussian curves were fitted separately to the net LVDT data due to each tunnel event. From the fitting results, two basic characteristics of the observed surface settlements can be concluded:

Characteristic 1: Larger S_{max} due to the second tunnel

As shown in Fig. 3, an increased magnitude of maximum surface settlement S_{max} can be intuitively observed in the second tunnel event when compared to the first.

Characteristic 2: Eccentricity of S_{max} for the second tunnel

In general, the surface settlement profile should be symmetrical and centred above the tunnel axis for a Greenfield excavation of a single tunnel. However, in Fig. 3, it is clear that the point of S_{max} for the second tunnel was drawn towards the first tunnel. The

offset from the second tunnel axis was termed as the "eccentricity (E) of S_{max}", which was expressed with the centre-to-centre tunnel spacing S. It is also interesting to note another fact from the Gaussian curve fitting that the eccentricity of S_{max} also existed in the first tunnel. This can only be attributed to the influence of the pre-existing second tunnel prior to the first tunnel event in the centrifuge tests.

In fact, characteristic 1 and characteristic 2 has been well recognised in previous numerical studies (Addenbrooke and Potts, 2001) and physical model tests (Chapman *et al*, 2007). They were usually considered as a consequence of the additional subsurface movements in the soil pillars between tunnels (or similarly the "overlapping zone" proposed by Hunt, 2005) caused by the second excavation in a sequential twin-tunnelling process. However, the mechanism by which the additional subsurface movements developed remained unclear. In this sense, detailed numerical modelling may be helpful, as it can provide a clear insight into the mechanism for the development of ground movements from a twin-tunnelling type operation.

3. NUMERICAL MODELS

Numerical analyses were carried out using commercial finite element software ABAQUS (version 6.14). A typical schematic drawing of the numerical model is shown in Fig. 4. The two-dimensional plane-strain model represented a complete section of the physical model (cf. Fig. 1). Roller boundaries were imposed on the both sides and

the base of the model to consider the well-greased condition on them in the centrifuge tests.

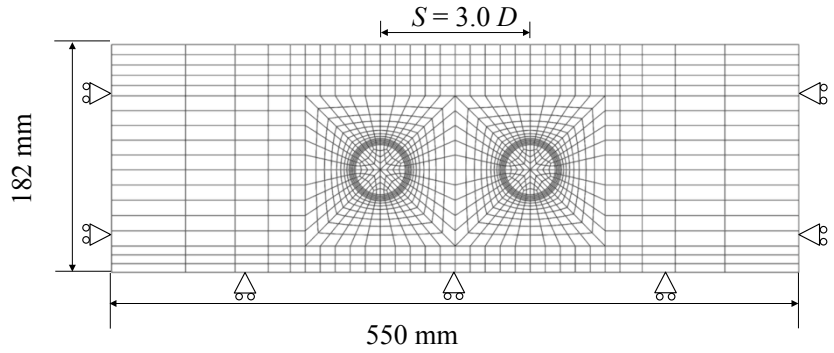

Fig. 4 Schematic of the numerical model (S = 3.0 D is shown as an example)

3.1 Simulation procedure

In order to realistically reproduce the load history, the simulation began from model preparation in analogy with the experimental procedure mentioned before, which includes 8 steps in total:

Step 1: Initial state (K_0 consolidation): The model was initiated by normally consolidated state. The effective vertical stress was set to 500 kPa and constant with depth; A K_0 = 1-sinφ' stress condition was adopted in equilibrium with applied surcharge of 500 kPa (cf. Fig. 5(a)).

Step 2 (One-dimensional swelling): The surcharge was reduced to 250 kPa, while the pore pressure of the entire model was kept zero, which corresponds to a fully consolidated process (cf. Fig. 5(b)).

Step 3 (Installing tunnels): At the very beginning of step 3, the surcharge was

deactivated, meanwhile, a -250 kPa pore pressure was imposed on all nodes of the model to achieve the same effective stress state as the one at the end of previous step; Subsequently, the soil in the two cavities was removed, and a total period of 4 hours was given for this step in accordance with the model making process (cf. Fig. 5(c)).

Step 4 (Consolidation in flight): Elastic water elements, with a density of 1000 kg/m^3, bulk modulus K_w of 2180 MPa as well as tiny shear modulus G_w, were activated in the cavities at the beginning of step 4. These water elements were predefined but deactivated in the previous three steps, which share the same nodes with the removed soil elements in step 3 (These water elements were general solid elements without the degree of pore pressure, therefore, there is no drainage from these water elements to the surrounding soil elements). Then the acceleration of gravity was increased to 100 *g* linearly in 4 minutes, followed by a sufficiently long time given for full consolidation. From this step, the bottom of the model was set completely permeable due to the drainage grooves there (cf. Fig. 5(d)).

Step 5 (First tunnel): "Water" elements inside the first tunnel were removed, meanwhile, a relatively small support pressure with a fixed gradient of 981 kPa/m along the depth was applied to the tunnel boundary to achieve a 3% volume loss within the same time period as in tests (60 seconds). (cf. Fig. 5(e)).

Step 6 (Consolidation after first tunnel): The "Water" elements were reactivated

inside the first tunnel at the beginning of step 6, followed by a time period of 180 seconds as a pause to represent a delay before the construction of the second tunnel. It should be noted that the "water" elements reactivated in this step were set free of gravity, which were employed only to undertake the unbalance force generated in the subsequent steps because all loads defined in the previous steps would be inherited in ABAQUS by default if without additional definitions (cf. Fig. 5(f)).

Step 7 (Second tunnel): Operations taken in step 5 for the first tunnel were repeated for the second (cf. Fig. 5(g)).

Step 8 (Consolidation after second tunnel): Operations taken in step 6 for the first tunnel were repeated for the second (cf. Fig. 5(h)).

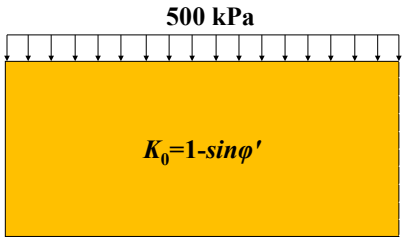

(a) K_0 Consolidation

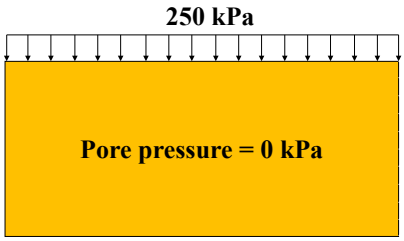

(b) One-dimensional swelling

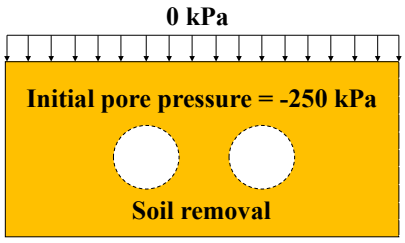

(c) Installing tunnels

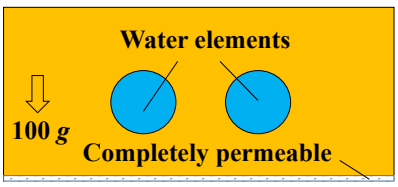

(d) Consolidation in flight

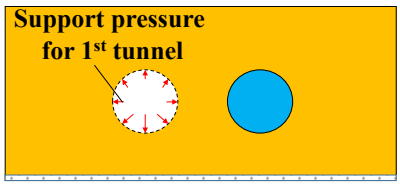

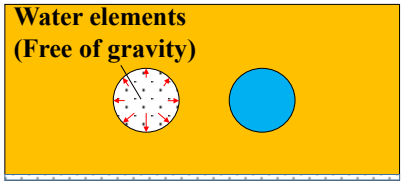

201

202 (e) First tunnel (f) Consolidation after first tunnel

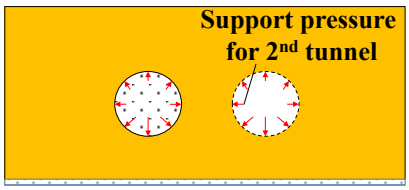

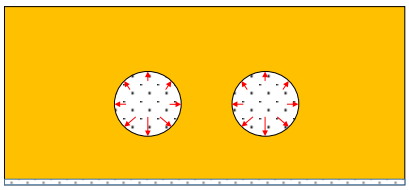

203

204 (g) Second tunnel (h) Consolidation after second tunnel

205 Fig.5 Simulation procedure for centrifuge tests (not scaled)

206 **3.2 Constitutive models**

207 Both Modified Cam Clay (MCC) model and Three-Surface Kinematic Hardening
208 (3-SKH) model were adopted in the numerical analyses. The 3-SKH model can be
209 considered as an extension of MCC model, which introduced two additional surfaces,
210 i.e., the yield surface (YS) and the history surface (HS) inside a MCC critical state
211 bounding surface (BS), as shown in Fig. 6. This makes it possible to simulate the
212 behaviour of soil over a wide range of strain levels as well as with changes of stress
213 path direction (Stallebrass, 1990).

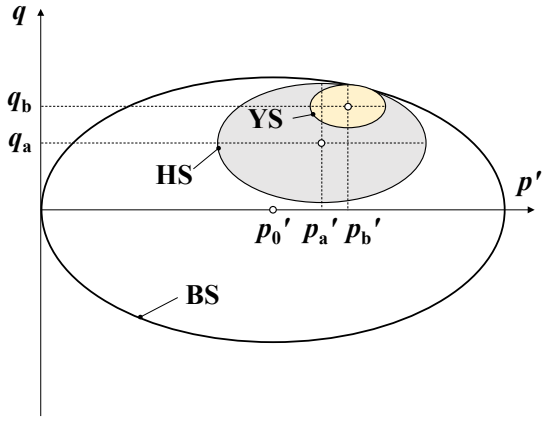

Fig. 6 Sketch of 3-SKH model in p'-q plane

The 3-SKH model was implemented using a user-defined material subroutine (UMAT), which was reprogrammed in FORTRAN language, following the original version used in CRISP by Stallebrass (1990) as well as the C++ version used in TOCHNOG by Masin (2004).

The soil parameters of Speswhite kaolin clay for both MCC and 3-SKH model have been well established after many calibration works by researchers at City, University of London, as shown in table 1.

Table 1 Soil parameters for both MCC and3-SKH model

MCC model (Morrison,1994)	M	λ	κ	e_{cs}	v				k_v mm/s	k_h mm/s
	0.89	0.18	0.035	1.97	0.3				4.7e-7	1.37e-6
3-SKH model (Stallebrass, 1990;Viggiani,1992)	M	λ^*	κ^*	e_{cs}	A kPa	T	S	ψ	k_v mm/s	k_h mm/s
	0.89	0.073	0.005	1.994	1964	0.25	0.08	2.5	4.7e-7	1.37e-6

4. VALIDATION OF NUMERICAL MODELS

Fig. 7 shows the computed and measured surface settlements. In general, both *MCC model and 3-SKH predicted wider and shallower settlement troughs when compared to the test data. Predictions closer to the test data might be obtained by* adjusting the parameters of the model. However, this is not undertaken in this study since the engineering properties of the used Speswhite kaolin clay have been well established due to the continuous input into the calibration (e.g., Stallebrass and Taylor, *1997; Grant, 1998; Masin, 2004; Bilotta and Stallebrass, 2009).*

It is clear to see that the 3-SKH model was capable of soundly reproducing the *two basic characteristics (Larger S_{max} and eccentricity of S_{max} in the second tunnel event) of the observed surface settlements in the centrifuge tests, whereas MCC model failed to provide those only except for the case with S = 1.5 D, which implied that the MCC* model might underestimate the interaction between the two tunnels.

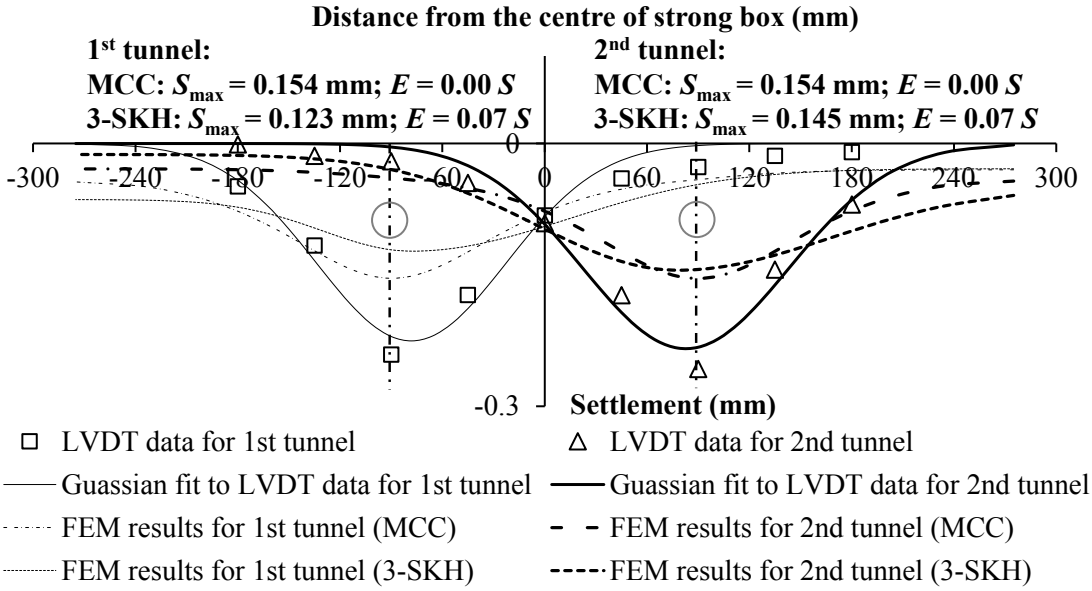

237

238 (a) S = 4.5 D

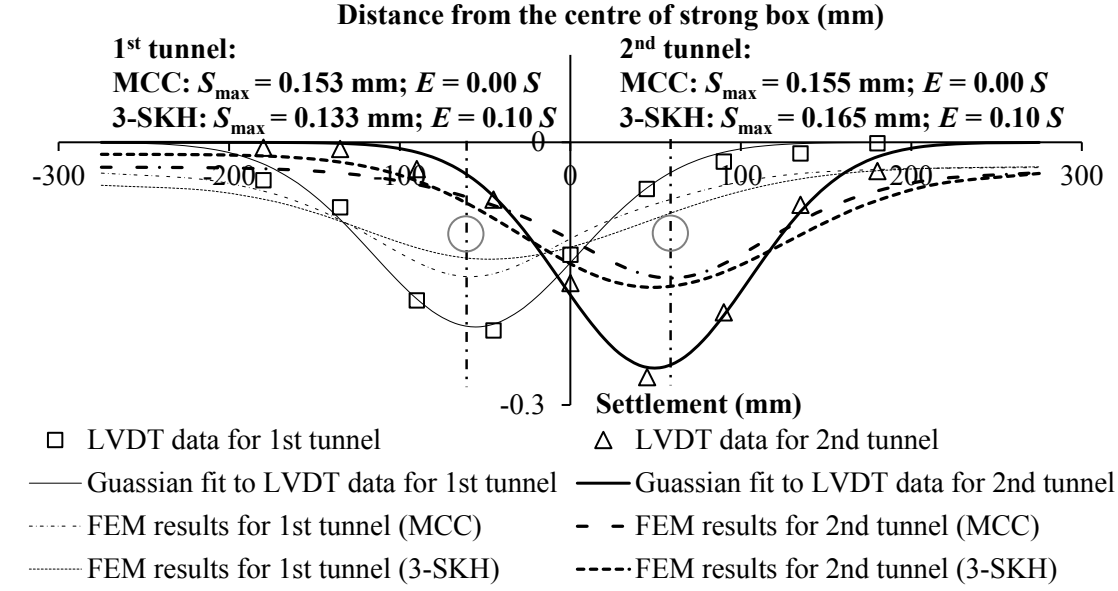

239

240 (b) S = 3.0 D

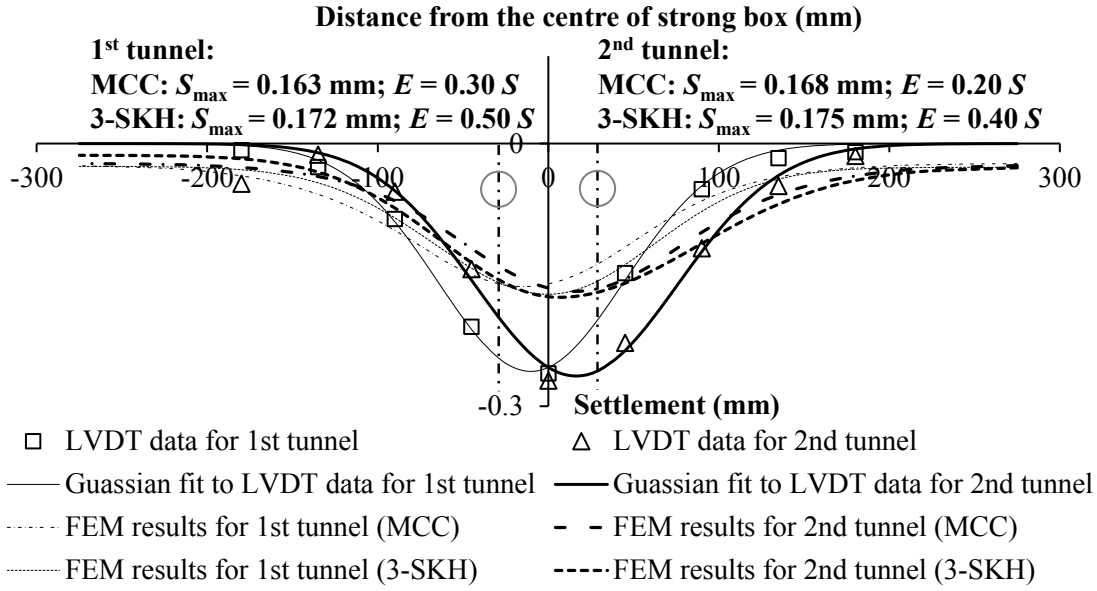

(c) S = 1.5 D

Fig. 7 Comparison of computed and measured surface settlements

Leaving aside the two basic characteristics mentioned above, it is interesting to note that in terms of magnitude of S_{max} and width of settlement trough, MCC model seemed better for the prediction of the first tunnel event for the case with S = 3.0 D and S = 4.5 D. To further examine the performance of both MCC model and 3-SKH model, comparison was also made between the computed and measured pore pressure changes at the midpoint between the two tunnels (cf. PPT in Fig. 1), as shown in Fig. 8 (PPT was absent in the test with S = 1.5 D). The PPT data in the tests with S = 3.0 D and S = 4.5 D showed similar regularity, which was seen to rise at the start of each tunnel event as a result of the arching effect (Kim et al, 1998; Lee, 2006), and then to drop before being stabilised due to consolidation. Basically, the changes in pore pressures predicted

by the 3-SKH model were very close to the observed PPT response as described above, while the results predicted by MCC model seemed quite imperceptible.

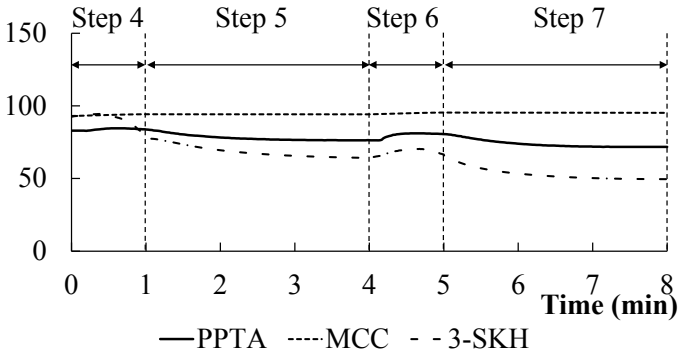

(a) $S = 4.5\ D$

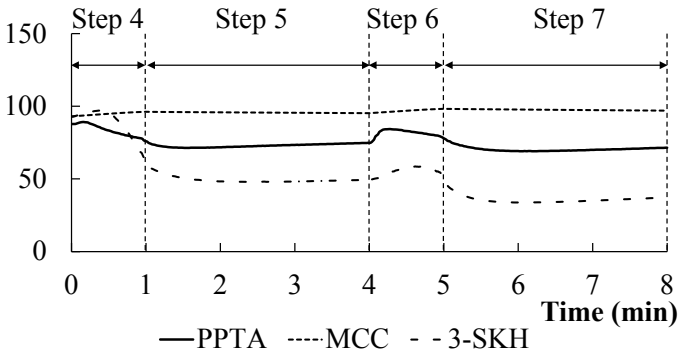

(b) $S = 3.0\ D$

Fig.8 Comparison of predicted and measured pore pressures

As greater changes in PPT readings may be relevant to more significant changes in effective stresses, the stress path at the same position predicted by both the MCC model and the 3-SKH model were also compared, as shown in Fig. 9. Considering the similar regularity, only the stress path in the test with $S = 3.0\ D$ is plotted.

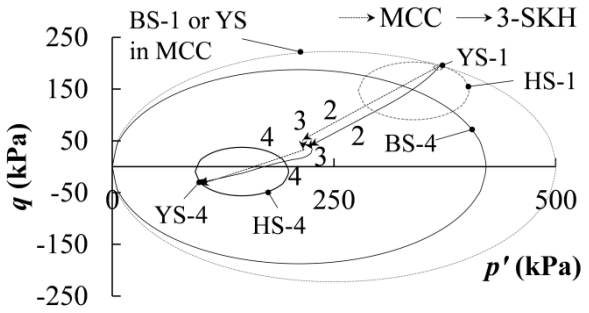

(a) Stress path from step 2 to 4 (both MCC and 3-SKH)

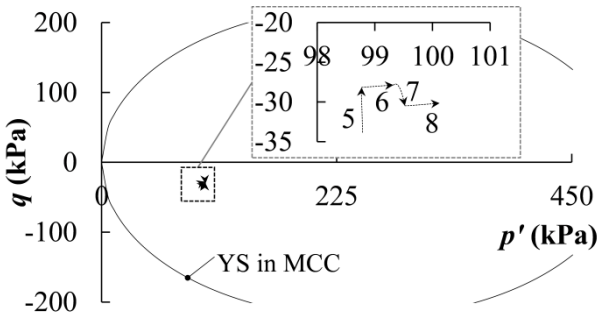

(b) Stress path from step 5 to 8 (MCC)

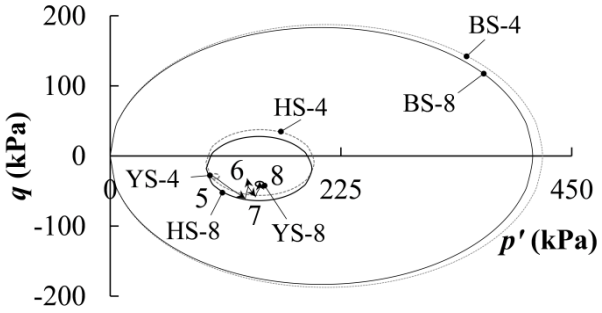

(c) Stress path from step 5 to 8 (3-SKH)

Fig. 9 Comparison of effective stress path predicted by MCC and 3-SKH model

The comparison began with the model preparation (step 2~4). As can be seen in Fig. 9(a), the two models work under different frameworks. The MCC model computed only elastic strains with a constant stiffness in a fixed yield surface (YS) during

unloading; while the 3-SKH model allowed plastic strains to develop inside a shrinking boundary surface (BS-1 shrunk to BS-4 at the end of step 4) in line with an increasing void ratio during swelling, and stiffness decrease due to the moving of both history surface (HS-1 to HS-4) and yield surface (YS-1 to YS-4). In general, the MCC model and 3-SKH model predicted similar stress path and almost the same stress state at the end of step 4, which means the MCC model may be satisfactory in providing good predictions for a monotonic unloading event.

Once the test began (step 5~8), the two models started to show distinct predictions for stress path (cf. Fig. 9(b) and Fig. 9(c)). The MCC model computed quite imperceptible stress variations compared to the 3-SKH model. This was due to the elastic assumption for the over consolidated soil around the excavated tunnel, which may lead to a very gentle change in effective stress at the monitoring point under a 3% volume loss. By contrast, the 3-SKH model could take the stress history into account, a much higher stiffness of soil was invoked due to a sudden change in the stress path direction (see the changes in stress path direction in step 4~8). This ensured a significant change in effective stress, and hence a comparable magnitude of changes in pore pressure as observed in the tests.

Therefore, in the simulation for a twin-tunnelling event, the MCC model may seem workable in predicting the surface settlements caused by the first tunnel, however,

294 would compute a less altered stress field. This may result in a significant
295 underestimation of the impact of a foregoing tunnel excavation on the surrounding soil,
296 and hence on the behaviour of the subsequent tunnel. By contrast, due to the superior
297 performance in modelling the non-linearity of soil stiffness dependent on stress history
298 in a multi-stage analysis, the predictions obtained using 3-SKH model for both surface
299 settlements and pore pressure changes were very close to the test data. As a
300 consequence, only the 3-SKH model is used in the following analyses to explain the
301 observed surface settlements in the centrifuge tests.

302 **5. EXPLANATION FOR OBSERVED SURFACE SETTLEMENTS IN**
303 **CENTRIFUGE TESTS**

304 As mentioned above, two basic characteristics (Larger S_{max} and eccentricity of S_{max}
305 in the second tunnel event) can be concluded from the observed surface settlements in
306 the centrifuge tests, which were both well reproduced by numerical simulation with the
307 3-SKH model.

308 In this section, two cases were simulated using the 3-SKH model for a comparison
309 of predictions with attempts made to explain the observed surface settlements. In Case
310 1 the analysis followed the same sequence of events as the centrifuge test with $S = 3.0$
311 D, for which both the procedures and the results of the simulation has been detailed in
312 previous sections. In contrast, case 2 refers to a virtual event, in which the only

difference from case 1 was that the volume loss in the first tunnel was set to 0% i.e. no unloading. Therefore, case 2 can be considered as an idealised case exclusive of the disturbance of the first tunnel to the soil prior to the second tunnel event. The results, obtained by subtracting the vertical displacements individually caused by the second tunnel in case 2 from the vertical displacements individually caused by the second tunnel in case 1, were termed as "additional settlements", which can be seen in Fig. 10 (Upheavals have been filtered out so as to clearly show the settlement zone).

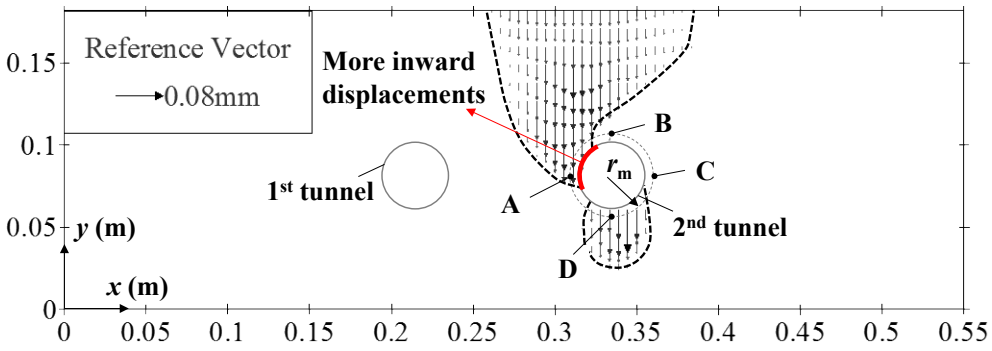

Fig. 10 Computed "additional settlements" due to 2nd tunnel

As illustrated in Fig. 10, "additional settlements" mainly arose on the left hand side (adjacent to the first tunnel) of the region above the second tunnel. With such a profile of "additional settlements", it is not difficult to understand both the increase in the magnitude of S_{max} and the eccentricity of S_{max} due to the second tunnel in case 1. Actually, this "additional settlement" profile was found stemming from the more inward displacements at the second tunnel springline closer to the first tunnel in case 1. Considering that the contraction mode of tunnel during excavation may rely on the

329 stiffness distribution of soil that surrounds the tunnel, four points in the vicinity of the
330 second tunnel (point A and C at tunnel springline, B at crown and D at invert) with a
331 distance r_m of 0.625D from the tunnel centre were chosen to compare the stress path
332 dependent stiffness of soil during the construction of the second tunnel in both case 1
333 and case 2.

334 Fig. 11 demonstrates the stress paths during the construction of the two tunnels at
335 the four points in both case 1 and case 2. Stress path 5, 6, 7 corresponded to step 5, 6
336 and 7 in case 1, respectively; while stress path 7′ referred to step 7 in case 2 (In case
337 2, the stress paths in step 5 and 6 were omitted since there were no changes in the
338 effective stress due to the zero volume loss in the first tunnel event).

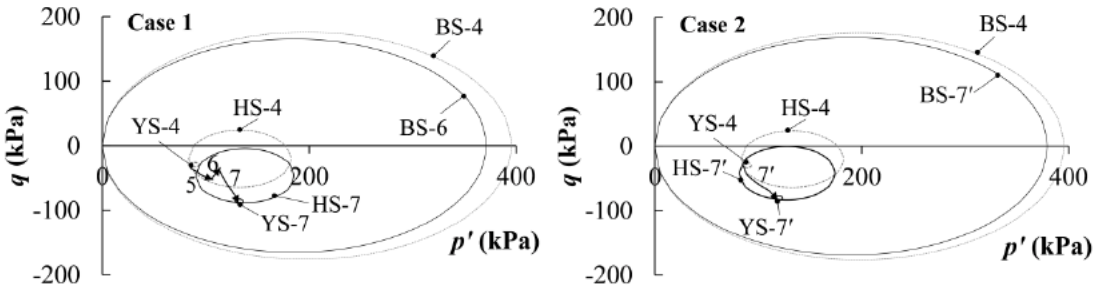

339

340 (a) Point A

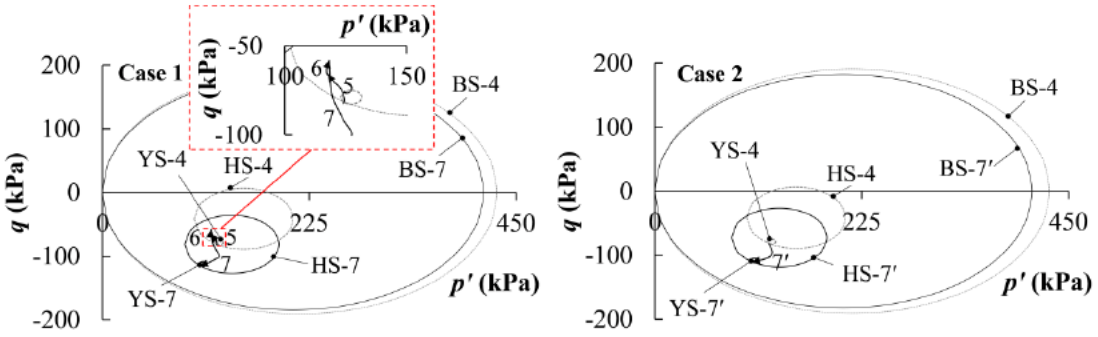

341

342 (b) Point B

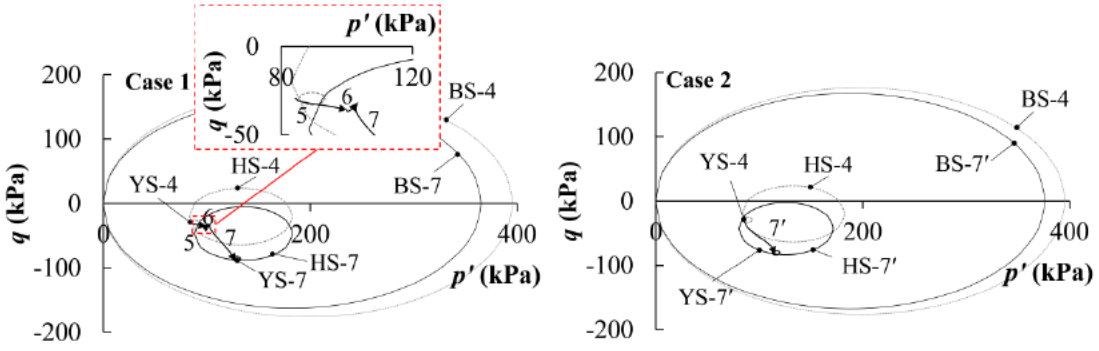

(c) Point C

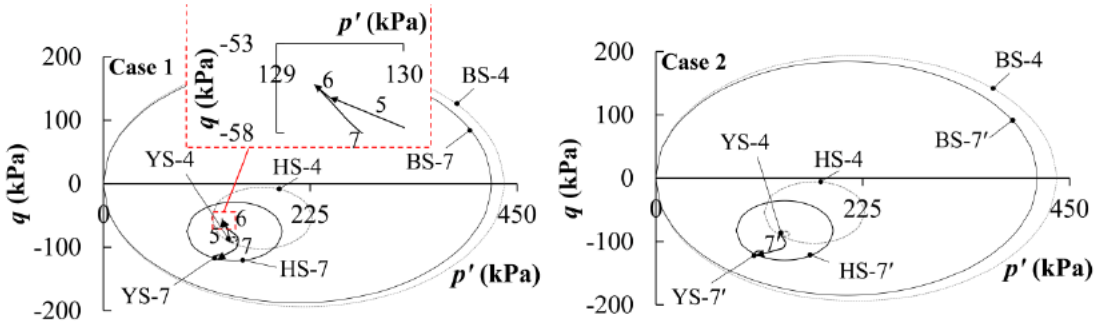

(d) Point D

Fig. 11 Comparison of stress paths at four typical points in both case 1 and case 2

During the construction of the second tunnel (step 7), the soil at the springline of the second tunnel (points A and C) was found to be subjected to a compression path (cf. stress path 7 and 7′ in Fig. 11(a) and Fig. 11(c)), whereas the soil at both the crown and invert of the second tunnel (Point B and D) followed an extension path (cf. stress path 7 and 7′ in Fig. 11(b) and Fig. 11(d)). Meanwhile, from the configuration of the kinematic surfaces at the end of step 7, all the history surfaces in the plotted figures were shown dragged down (HS-4 to HS-7) following an increase in deviatoric stress q

356 (absolute value), which meant the conjugate point of the stress point on the history
357 surfaces in stress path 7 (or 7′) were located at the bottom half of the surfaces.

358 In case 1, due to the first tunnel, the stress history at point A and C prior to the
359 second tunnel (stress path 5 and 6) mainly experienced an increase in deviatoric stress
360 q, which may shorten the distance from the stress point to its conjugate point on the
361 history surface in the following stress path (stress path 7); while the stress history (stress
362 path 5 and 6) at point B and D exhibited a decrease in deviatoric stress q, which may
363 separate the stress point from its conjugate point on the history surface in the
364 forthcoming stress path. According to the hardening rule of the 3-SKH model, the
365 stiffness of soil at a yielded state is relevant to the distance between the stress point and
366 its conjugate point on the history surface, generally, a larger distance contributes to a
367 higher stiffness. Therefore, in the second tunnel, different responses of soil stiffness at
368 the four points would be expected for the two cases, which can be seen in Fig. 12.

369 Following Atkinson *et al.*(1990) and Stallebrass (1990), the notation G_c' was
370 adopted in this paper to define the tangential shear modulus, which was obtained by

371 $$G_c' = \frac{1}{3}\left|\frac{dq}{d\varepsilon_s}\right| \tag{1}$$

372 Where ε_s is shear strain and defined as

373 $$\varepsilon_s = \sqrt{\frac{2}{9}\left\{\left(\varepsilon_x-\varepsilon_y\right)^2+\left(\varepsilon_y-\varepsilon_z\right)^2+\left(\varepsilon_x-\varepsilon_z\right)^2+6\left(\varepsilon_{xy}{}^2+\varepsilon_{xz}{}^2+\varepsilon_{yz}{}^2\right)\right\}} \tag{2}$$

374 To explain the greater volume loss into the second tunnel, Addenbrooke and Potts
375 (2001) clarified that the excavation of the first tunnel would reduce the stiffness of the
376 soil in which the second tunnel was then excavated. However, from Fig. 12, it is clear
377 to see that the response of soil stiffness around the second tunnel was not consistently
378 softening due to the excavation of the first tunnel. Actually, the response was found to
379 be highly dependent on the relative changes of the stress path in the two tunnel events.
380 From the comparison of G_c' in case 1 and case 2, due to the first tunnel, the soil at the
381 springline of the second tunnel (point A and C) softened, while the soil at both tunnel
382 crown and invert hardened. The effect of recent stress history on shear stiffness
383 decreased as the soil is loaded and vanished with the increase of deviatoric stress q. It
384 is the different shear stiffness at the beginning of the second tunnel event which is most
385 significant. To quantify the softening of soil at point A and C, as well as the hardening
386 of soil at point B and D due to the first tunnel, the secant shear modulus with a notation
387 of G_s' was used in this paper, which was denoted as

388 $$G_s' = \left| \frac{\Delta q}{\Delta \varepsilon_s} \right| \tag{3}$$

389 Where Δq and $\Delta \varepsilon_s$ were the change in deviatoric stress and shear strain during tunnel
390 construction, respectively.

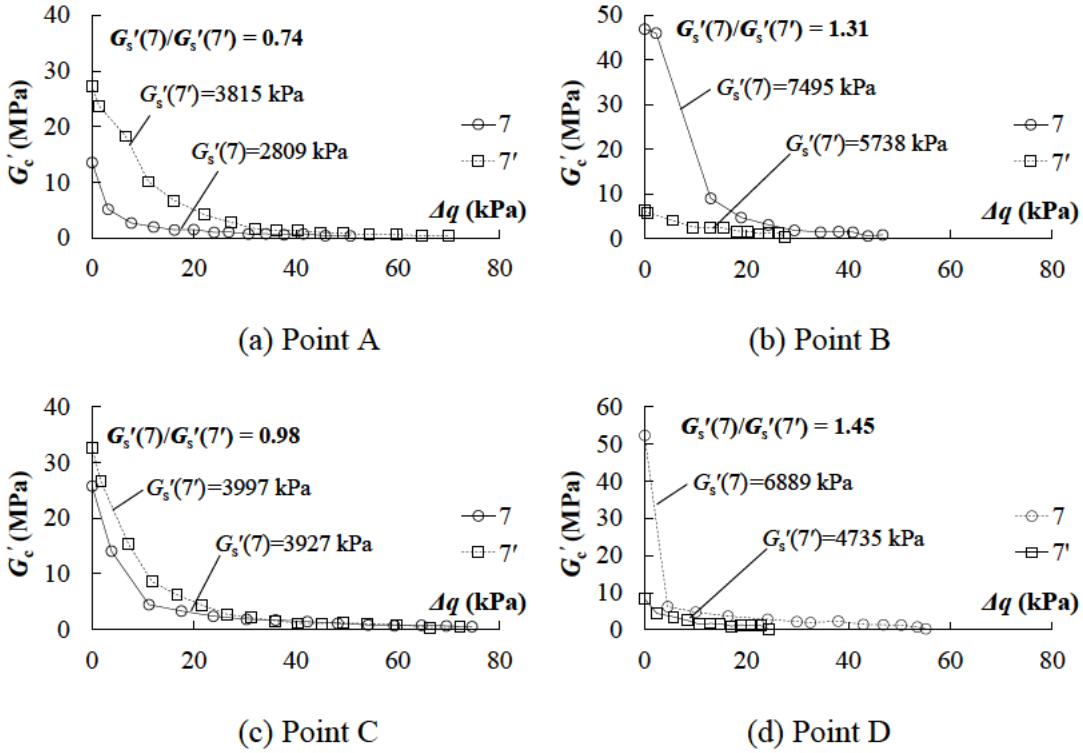

(a) Point A (b) Point B

(c) Point C (d) Point D

Fig. 12 Comparison of soil stiffness during step 7 in both case 1 and case 2

From the comparison of G_s' in case 1 and case 2, the softening effect on soil at point A due to the first tunnel was found more significant than that at point C. This was because point A was closer to the first tunnel and may suffer from stronger disturbance. In view of this, as the tunnels were supported by water in the tests, the reduction of the support pressure all around the cavity during tunnelling should be the same. Hence, under the same volume loss (3%), the soil in the region near point B was expected to displace more towards the second tunnel as it was much softer than other regions, and accordingly more settlements would be induced in the soil pillars between the two tunnels, by which the observed surface settlements can be explained.

6. CONCLUSIONS

This study investigated the ground surface settlements induced by sequential twin tunnelling in over consolidated clay. Credible centrifuge tests were presented first to show the two basic characteristics of the surface settlements due to a twin-tunnelling type operation, which were then investigated in detail through the use of both the Modified Cam Clay model (MCC) and the Three-Surface Kinematic Hardening Model (3-SKH) in the numerical simulation.

The computations using the MCC model could not reproduce the two key characteristics of the observed surface settlements in the centrifuge tests. Through a further comparison of the prediction with the pore pressure transducer (PPT) data, the main reason for the poor performance of the MCC model was addressed. It was demonstrated that the assumption of elastic response inside the yield surface may under predict the variations in soil stress around the tunnels, and hence underestimate the interaction between the two tunnels. By contrast, the 3-SKH model would invoke a high stiffness if a sudden change in stress path direction was detected in a multi-staged simulation, which guaranteed considerable changes in soil stress during the construction of the two tunnels, highlighting the importance of improving the predictions with the effects of previous stress history on the subsequent stiffness of soil to be modelled.

Under the theoretical framework of the 3-SKH model, the two characteristics of the observed surface settlements can be successfully explained. Numerical results indicated that the first tunnel may change the stiffness of the soil around the second tunnel, which was found associated with the relative changes of stress path in the two tunnel events. Due to the first tunnel, it was demonstrated that the soil at the springline of the second tunnel was softened, whereas the soil at both the crown and invert was hardened. In particular, the softening of soil at the springline adjacent to the first tunnel was most significant. This may cause an asymmetrical contraction of the second tunnel during excavation with more inward displacements observed on the softer side, and more settlements would be induced in the soil pillar between the two tunnels, which resulted in an increase in the magnitude of S_{max} and an eccentricity of S_{max} observed in the second tunnel event.

ACKNOWLEDGEMENTS

The authors would like to acknowledge the financial support from the National Key R&D Program of China (Grant No. 2017YFC0805407), the National Natural Science Foundation of China (Grant No. 41630641), the National Natural Science Foundation of China (Grant No. 51808387), and the National Key R&D Program of China (Grant No. 2016YFC0802008).

REFERENCES

Addenbrooke, T.I., 1996. Numerical analysis of tunnelling in stiff clay. Ph.D. thesis, University of London.

Addenbrooke T. and Potts D.M. (2001). Twin tunnel interaction: surface and subsurface effects. International Journal of Geomechanics 1(2): 249-271.

Atkinson, J. H., Richardson, D. and Stallebrass, S. E. (1990). Effect of recent stress history on the stiffness of overconsolidated soil. Géotechnique. 40(4): 531-40.

Bilotta E. and Stallebrass S.E. (2009). Prediction of stresses and strains around model tunnels with adjacent embedded walls in overconsolidated clay. Computers and Geotechnics. 36: 1049-57.

Chapman D.N., Ahn S.K., Hunt D.V.L. (2007). Investigating ground movements caused by the constrution of multiple tunnels in soft ground using laboratory model tests. Canadian Geotechnical Journal. 44:631-643.

Cooper M.L. and Chapman D.N. (1998). "Movements of the Piccadilly Line tunnels caused by the new Heathrow Express tunnels". Proc. of the World Tunnel Congress′ 98 on tunnels and metropolises, Sao Paulo, Brazil, pp. 294-254. Balkema.

Cooper, M.L., Chapman, D.N., Roger, C.D.F., Chan, A.H.C., 2002. Movements of the Piccadilly Line tunnels due to Heathrow Express construction. Géotechnique 52 (4), 243-257.

Cording E.J. and Hansmire W.H. (1975). "Displacement around soft tunnels". Proc. 5th

Pam-Am Conf. on Soil Mech. and Found. Engineering, Buenos Aires, Vol. 4, pp. 571-633.

Divall S. and Goodey R.J. (2012). Novel apparatus for generating ground movements around sequential twin tunnels in over-consolidated clay. Online publication by Proceedings of the ICE: Geotechnical Engineering, 10-11.

Divall S. (2013). Ground Movements Associated with Twin-tunnel Construction in Clay. PhD thesis, City University London, London, UK.

Divall, S. and Goodey, R.J. (2015). Twin-tunnelling-induced ground movements in clay. Proceedings of the Institution of Civil Engineers: Geotechnical Engineering, 168(3), pp. 247-256.

Fargnoli, V., Boldini, D., Amorosi, A., 2015. Twin tunnel excavation in coarse grained soils: observations and numerical back-predictions under free field conditions and in presence of a surface structure. Tunnelling and Underground Space Technology 49, 454-469.

Grant, R.J. (1998). Movements around a tunnel in two-layer ground. Ph.D. Thesis, City University London.

Hunt D.V.L. (2005). Predicting the ground movements above twin tunnels constructed in london clay. PhD thesis, University of Birmingham, Birmingham, UK.

Kim S. H., Burd H. J., and Milligan G.W.E. (1998). Model testing of closely spaced

tunnels in clay. Géotechnique. 48(48):375–88.

Lee C.J., Wu B.R., Chen H.T., Chiang K.H. (2006). Tunnel stability and arching effects during tunneling in soft clayey soil. Tunnelling and Underground Space Technology. 21: 119-32.

Mair, R.J. (1979). Centrifugal modelling of tunnel construction in soft clay. PhD thesis, University of Cambridge, Cambridge, UK.

Masin D. (2004). Laboratory and Numerical Modelling of Natural Clays. MPhil thesis, City University, London, UK.

Morrison, P. R. J. (1994). Performance of foundations in a rising groundwater environment. PhD thesis, City University, London, UK.

Nyren R. (1998). Field Measurements Above Twin Tunnels in London Clay. PhD thesis, Imperial College London, UK.

O'Reilly M.P. and New B.M., (1982). Settlements above tunnels in the United Kingdom - their magnitude and prediction, Tunnelling′ 82, Papers presented at the 3rd International Symposium, Inst of Mining and Metallurgy, London, England, pp. 173-181.

Peck, R.B. Deep excavations and tunnelling in soft ground. Proc. 7th ICSMFE. 1969; 225–90.

Roscoe K.H. and Burland J.B. (1968). On the generalised stress–strain behaviour of a

‘wet’ clay, in engineering plasticity. In: Heyman, Leckie, editors, pp. 535–609.

Schofield A.N. (1980). Cambridge geotechnical centrifuge operations. Géotechnique. 30(3):227–68.

Stallebrass S. E. (1990). The effect of recent stress history on the deformation of overconsolidated soils. PhD thesis, City University, London, UK.

Stallebrass S.E. and Taylor R.N. (1997). The development and evaluation of a constitutive model for the prediction of ground movements in overconsolidated clay. Géotechnique. 47(2):235–53.

Taylor R.N. (1984). Ground movements associated with tunnels and trenches. PhD thesis, University of Cambridge, Cambridge, UK.

Viggiani, G. (1992). Small strain shear stiffness of fine grained soils. PhD thesis, City University, London, UK.